Check for updates

A first run-of-river hydropower plant development in a permafrost-rich subarctic Canadian region: short-term fate of mercury and carbon

Mariane St-Aubin,[a] Jean-François Lapierre,[a] Dominic E. Ponton, [iD][a] Michel Sliger,[b] Jeanne Gaudreault,[c] Éric Atagotaaluk,[d] Daniel Fortier [iD][b] and Marc Amyot [iD] *[a]

A first run-of-river power plant built in Nunavik (QC, Canada) lies in a continuous permafrost zone, a substantial carbon (C) rich mercury (Hg) reservoir. Its impoundment could promote permafrost thaw and remobilize Hg and lead to the enhanced production of highly toxic methylmercury (MeHg). To elucidate how RORs can influence C and Hg dynamics and transformations in a subarctic landscape, soils, water and benthic invertebrates were sampled shortly before and after the flooding. Soil Hg concentrations were higher in the organic active layer than in frozen ground. Three months after river impoundment, MeHg concentrations and proportions in the surface organic layer of flooded soils were seven and four times higher, respectively. A similar increase was observed in surface waters of the newly created bay, where MeHg concentration and proportion were, respectively, ~10 and four times higher. Biological MeHg concentrations increased in low trophic level organisms associated with this flooded environment, namely primary consumers (~4×) and omnivores (~3×). However, these rises were limited to the small (<1 km^2) newly created bay, highlighting spatial heterogeneity in the production and trophic transfer of MeHg at the river scale in response to recent impoundment.

Environmental significance

Small hydropower plants account for more than 90% of global hydropower installed capacity but few studies have investigated their environmental impact even though it could be larger per megawatt produced than large hydroelectric dams. Mercury can be transformed to the neurotoxic methylmercury (MeHg) when soils are flooded by powerplant impoundments and can then be bioaccumulated and biomagnified in foodwebs. In the North, such flooding can occur in permafrost-rich areas with unknown consequences on Hg cycling. A first hydropower plant was recently built in the northern Canadian subarctic region to provide a sustainable energy source to an Inuit community. This study provides the first account of the environmental impact of subarctic powerplants on mercury cycling for communities consuming freshwater fish.

Introduction

Standing as a leading renewable energy source worldwide, hydropower is broadly supported by national incentives and policies aimed to mitigate global carbon (C) emissions.[1] Many parts of the world witness an unprecedented proliferation of small hydropower plants (SHP) (generally defined as <10 MW) like run-of-the-river (RORs) dams, notably to sustain isolated communities that rely solely on fossil fuels.[2,3] While it is widely accepted that large reservoirs can impact mercury (Hg) and C cycling, less is known on SHP impacts on the latter, let alone in remote northern landscapes featured with permafrost.[4,5] Known environmental impacts of river damming include the flooding of terrestrial soils which creates niches for the microbial transformation of Hg into methylmercury (MeHg), a potent neurotoxin that bioaccumulates and biomagnifies along aquatic food chains.[6] In northern regions, large boreal reservoir dams cause a temporary surge of MeHg in top predators that may persist up to 30 years before returning to pre-flooding levels.[7] Data about Hg cycling in SHP is scarce despite the fact they account for 91.5% of global hydropower installed capacity.[8] The few existing studies in southern rivers showed that RORs had little to no significant impact on Hg and MeHg levels in wildlife and water.[9–11] In contrast, within a boreal watershed impacted by multiple disturbances affecting the mobilization of organic matter (OM) and mercury (Hg), elevated concentrations of methylmercury (MeHg) were detected in flooded areas upstream of two run-of-river (ROR) structures—across sediments, the water column, biofilms, and throughout the entire food web.[12–14]

[a]*Groupe de Recherche Interuniversitaire and Limnologie (GRIL), Département des Sciences Biologiques, Université de Montréal (UdeM), 1375 Thérèse-Lavoie-Roux Ave., Montréal, Québec H2V 0B3, Canada. E-mail: m.amyot@umontreal.ca*

[b]*Département de Géographie, Université de Montréal (UdeM), 1375 Thérèse-Lavoie-Roux Ave., Montréal, Québec H2V 0B3, Canada*

[c]*Innergex Renewable Energy, 1225 Saint-Charles West Street, Longueuil, Quebec J4K 0B9, Canada*

[d]*Pituvik Landholding Corporation, P.O. Box 285, Inukjuak, Quebec J0M 1M0, Canada*

3572 | *Environ. Sci.: Processes Impacts*, 2025, **27**, 3572–3585

This journal is © The Royal Society of Chemistry 2025

Long-range atmospheric transport of Hg followed by deposition has caused an accumulation of Hg in northern ecosystems since the industrial revolution, but also at longer temporal scales.[15] C-rich permafrost and its active layer are presumed Hg reservoirs that could store between 597 Gg Hg to 1656 Gg Hg, accounting for up to 67% of global Hg reservoirs.[16,17] In the pedosphere, Hg distribution is largely explained by soil's OM content as it offers preferential binding sites.[18] Through runoff, erosion, and leaching, soil Hg and MeHg can be co-mobilized with dissolved organic matter (DOM) to the surrounding aquatic ecosystems, where OM optical indicators for terrestrial origins such as humic-like material have shown in some cases to be strong predictors of Hg concentrations in surface waters.[19–21] Undergoing global permafrost degradation is likely to enhance mobilization of C-bound Hg in receiving waters.[22–24] These DOM exports could exhibit a unique fingerprint, hence a changing radiocarbon age as well as a strong dominance of colored DOM linked with land-derived C.[25–28] The impoundment related to a hydroelectrical development in a permafrost covered region can potentially impact its thermal regime and initiate or accelerate its degradation, as observed during seasonal floods or under river beds, which could locally lead to a similar portrait in surface waters.[29] Moreover, the flooding of fresh OM could lead to changes in carbon sources for the biota and shifts in MeHg trophic magnification efficiency.[13] Stable isotopic tools like $\delta^{13}C$ and $\delta^{15}N$ are largely applied tools to follow up on Hg dynamics in food webs, as they, respectively, give insight on diet sources and trophic level.[30] However, no field study previously focused on ROR impacts on Hg and C cycling from soils to the food chain, in a subarctic environment.

Innavik Project, a 7.5 MW ROR, now provides Inukjuak (Nunavik, Quebec, Canada) with renewable energy, making it the first Inuit community of Nunavik to partly dissociate from fossil fuels for domestic use (details of this project can be obtained at **https://innavikhydro.com**). Our objectives were to (1) assess the short-term impacts of flooding on Hg and MeHg soil concentrations; (2) evaluate the effects of flooding on DOM and Hg exports from the flooded area paired with radiocarbon dating and optical assessments of dissolved organic carbon (DOC), a proxy for DOM and (3) establish baseline and short-term influences of flooding on an aquatic food web MeHg contamination using stable isotopic analyses.

Material and methods

Study design and study area

Innavik Hydro is located 10 km upstream from the river mouth of the 300 km long Innuksuac River (58.5 N, −78.0 W), Nunavik (Quebec, Canada), which drains 11 370 km² before reaching the Hudson Bay at an average flow of 100 m³ s⁻¹.[31] The final stage of deglaciation of the eastern coast of Hudson Bay occurred around 8.47 ka BP.[32] The Inukjuak sector was then covered by ice-contact, sub-aquatic, outwash sands.[32] During the marine regression, marine terraces raised and beaches were formed and these deposits were dissected by fluvial incision forming river terraces during subsequent land emergence.[33] The study area lies in the subarctic continuous permafrost zones[34] and the

mean annual air temperature was −5.63 °C for the period 2008–2018.[35] Most of the permafrost in the study area is epigenetic, with a temperature around −3 °C and an active layer thickness ranging between 1 and 1.5 m.[35] The impoundment of the Innuksuac River in June 2023 created a headpond of 1.13 km², of which 0.65 km² was flooded land, leading to the disappearance of three rapids and the creation of a new bay.[31]

Four sampling campaigns took place from June 2022 to October 2023, where water was sampled in four sectors, namely the riverine portion (HPR; $n = 2$) and the newly formed bay (HPB; $n = 2$) of the headpond, the fluvial lake Qataakuluup Tashinga upstream from the flooded area (QT; $n = 1$), and downstream from the ROR (DWST; $n = 5$). Depending on local constraints, not all water sites were sampled at each campaign. In June 2023, an additional systematic water sampling was performed downstream from the plant to monitor water quality changes during the first days of the initial impoundment (June 22 to 30, 2023). Additionally, during the campaigns of September 2022 and October 2023, pre-flood soil pedons ($n = 9$) and post-flood soil cores ($n = 9$), respectively, were collected in the bay area, while benthic invertebrates and small fishes were collected at some of the water sampling sites under pre-flood ($n = 4$) and post-flood ($n = 5$) conditions (Fig. 1).

Field sampling

We followed a trace metal sampling procedure,[36] and all suitable materials were priorly acid-washed with trace metal grade 10% HCl (volume/volume (v/v)). Prior to the impoundment, pedons were characterized and sampled in the soon-to-be flooded bay, with a focus on horizons and frost front depths. A sample of each horizon was collected with a graded syringe in a Whirl-Pak® bag. Flooded soils were collected with a stainless and galvanized steel corer (radius = 10 cm, length = 25 cm), and sub-samples at 5, 10 and 15 cm at the center of each core were bagged. All soil samples were kept at −20 °C then weighed before and after being freeze-dried (Freeze-Dry System, Labconco) and homogenized with a glass rod.

At each site, water quality (i.e. pH, temperature and turbidity) was measured with either an EXO3 Multiparameter Sonde or a YSI ProDSS. Water samples were collected from the shore (depth ± 0.5 m) using a site-conditioned peristaltic pump with a Teflon tubing within a Norprene tube and a 0.45 μm metal-free filtration cartridge for filtered samples. Site-conditioned amber glass bottles were used for mercury (Hg) and dissolved organic carbon (DOC) analyses and collected in triplicate. A 550 °C pre-combusted GF/F microfiber filter and QM-A quartz microfiber filter were respectively used to collect suspended particulate matter (SPM) and particulate organic carbon (POC) for ¹⁴C analyses, and the volume filtered was used to calculate concentrations. For DOC radiocarbon analyses, filtered water was collected in 500 mL polycarbonate bottles. Hg and DOC samples were kept in the dark at 4 °C while ¹⁴C DOC and filters were kept at −20 °C until analyses. Samples for Hg were spiked at 0.4% HCl (v/v). A field blank was performed with Milli-Q water at the end of each day to examine for possible contamination.

This journal is © The Royal Society of Chemistry 2025

Environ. Sci.: Processes Impacts, 2025, **27**, 3572–3585 | **3573**
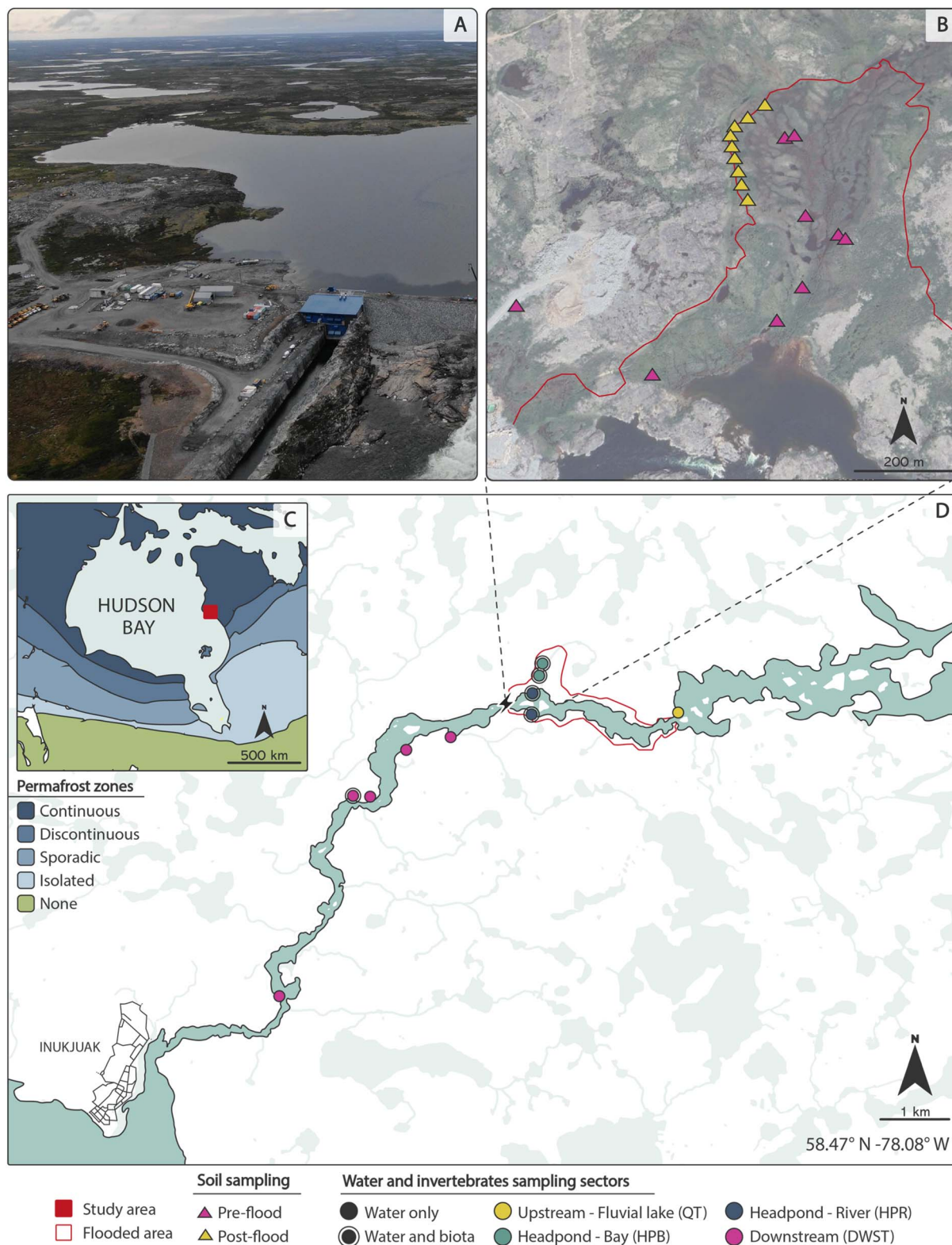
Fig. 1 Map of the study area with (A) the new flooded bay, (B) the sampling sites for soils in the new flooded bay, (C) the location of the study with regard to the permafrost zones[39] and (D) the sampling stations for water and biota.

Benthic invertebrates and small fishes (<10 cm) were collected in the sediments and overlying water with a kick net. All invertebrates were identified and sorted to the family rank apart from the sub-class Oligochaeta. A total of 12 families and one sub-class of invertebrates were found, from primary consumers to predators (Table S1). Similar size organisms of a given taxon were pooled together to ensure enough biomass for analyses. All organisms were depurated of their gut content

3574 | Environ. Sci.: Processes Impacts, 2025, 27, 3572–3585

This journal is © The Royal Society of Chemistry 2025

in site water for 24 h. Before analysis, shells and cases were removed for mollusks and caddisflies. Four species of small fish, juvenile slimy sculpins (*Cottus cognatus*), three and nine spined sticklebacks (*Gasterosteus aculeatus*, *Pungitius pungitius*), and Cyprinidae sp., were collected according to the protocol 22-100 approved by the Comité de déontologie de l'expérimentation sur les animaux from the University of Montreal. Biological samples were kept at −20 °C, then freeze-dried and homogenized with a glass rod.

Laboratory analyses

For Hg and MeHg analyses, blanks, fresh standard solutions and certified reference material (CRM) were ran every 10–14 samples to ensure instrument performance and stability (Table S2). Total Hg (THg) measurements in soils were performed by atomic absorption spectrometry with a DMA-80© Milestone Direct Mercury Analyzer using the United States Environment Protection Agency (US EPA) 7473 method,[37] while filtered and unfiltered THg in water was analyzed using a Tekran 2600 cold vapor atomic fluorescence spectrometer (CVAFS) following the US EPA 1631 method.[38] All methylmercury (MeHg) analyses were conducted with a Tekran 2700 CVAFS using the US EPA 1630 method[39] with sample pre-treatments depending on the type of analyte. Filtered and unfiltered water samples were priorly distilled,[40] soil samples were priorly digested in a 25% (w/v) KOH–methanol mixture, while invertebrates and small fish were digested overnight at 65 °C in 0.5 or 1 mL of HNO_3 (3 M).

The proportion of organic matter content (% OM) in soils was analyzed by loss on ignition.[41] Samples with >30% OM were classified as organic while the rest was sorted as mineral.[42] DOC concentration in water was measured with a Sievers M5310C TOC Analyzer following the US EPA 415.1 method,[43] within the week following the field sampling. DOC absorbance was measured using a UV-visible Cary 100 spectrophotometer© Agilent Technologies (250–800 nm) and fluorescence was measured using a Cary Eclipse fluorescence spectrophotometer© Agilent Technologies. Excitation–emission matrices were built from excitation from 230 to 450 nm (5 nm increments), and emission was recorded from 240 to 600 nm (2 nm increments). Matlab was used to generate a five-component PARAFAC model and data correction is detailed in the study by De Bonville *et al.* (2020).[44] PARAFAC components were compared with published studies on the online repository OpenFluor database and only matches with a minimum similarity of 0.95 were kept.[45] Briefly, C1, C2 and C4 components represent humic-like terrestrial derived material while C5 is protein-like and C3 stands for microbially derived humic-like material (Table S3).[46]

The radiocarbon dating of DOC and POC was performed in pretreated samples using an Ionplus AG© Mini Carbon Dating System (MICADAS) (Dietikon, Zurich, Switzerland).[47–49] The $\delta^{13}C$ and $\delta^{15}N$ analyses were conducted using a Micromass© Isoprime 100 (Elementar UK Ltd, Cheadle, UK) isotope ratio mass spectrometer coupled to an Elementar© Vario MicroCube (Elementar UK Ltd, Cheadle, UK) elemental analyser in continuous

flow mode. The results were normalized using reference materials which led to analytical uncertainties of $\pm0.1‰$ for $\delta^{13}C$ and $\pm 0.2‰$ for $\delta^{15}N$. No significant difference was observed among taxa $\delta^{15}N$ from the same trophic group (*i.e.* Kruskal–Wallis test, primary consumer: $p = 0.1897$; omnivore: $p = 0.6377$ and predator), hence all organisms within the same category were grouped for further investigations. The trophic magnification slope (TMS), frequently used to assess MeHg trophic transfer efficiency, was estimated as the slope (b) of the regression between (log)MeHg and $\delta^{15}N$ signatures while the trophic magnification factor (TMF) corresponds to $10^{(b\times3.4)}$.[6]

Statistical analysis

Statistical analysis was carried out using JMP 18 software. The significance level for all tests was set at $p < 0,05$ and classified as $p < 0.05$, $p < 0.01$, $p < 0.001$. Log-transformations were used when the data did not meet the criteria for parametric tests (*i.e.* normal distribution and homogeneity of variances), and non-parametric equivalent tests were used if the distributions still did not meet normality. Thus, correlations were assessed with Pearson or Spearman coefficient while groups were compared with Student's *t*-test or Wilcoxon test. To validate our simple linear regression models, we ensured that the residuals were normally distributed.

Results and discussion

Impoundment increased methylmercury concentrations in the top organic layer

Total mercury (THg) measured in pre-flood soils was almost exclusively found in the 11–27 cm thick superficial organic layer (186 ± 61 ng g_{dw}^{-1}), which was part of the active layer of the permafrost as the frozen ground was found at depths ranging from 72 to 164 cm (Fig. S1). The organic matter (OM) content of soil highly influenced the distribution of THg ($R^2 = 0.64$, $p < 0.0001$), while the average ratio of mercury to carbon (R_{HgC}) was 0.26 ± 0.17 µg Hg per g C. Methylmercury (MeHg) was also predominant in the organic soils (0.96 ± 0.66 ng g_{dw}^{-1}), where it constituted 0.05% to 2.8% of THg (% MeHg). In contrast, the mineral A- and B-horizons showed low concentrations of THg (10 ± 18 ng g_{dw}^{-1}) and MeHg (0.09 ± 0.05 ng g_{dw}^{-1}).

Three months post-impoundment, average soil THg concentrations persisted within the same range (Wilcoxon test, $p = 0.095$), averaging 210 ± 87 ng g_{dw}^{-1} in the organic soils and 28 ± 56 ng g_{dw}^{-1} in the mineral ones. MeHg concentrations increased by 681% within the same time in the organic layer compared to background levels (Wilcoxon test, $p = 0.003$). A wider range of MeHg concentrations in the organic compartment was also measured following impoundment, with maximal concentrations as high as 26 ng g_{dw}^{-1} consistently found at the uppermost centimeters of each core (Fig. 2). Throughout the event, soil THg remained a strong predictor for MeHg, yet the slope of the linear regression doubled post-impoundment (Fig. 2). In addition to this rapid upsurge in MeHg concentrations, the % MeHg, often used as a proxy of net methylation efficiency in substrates,[50,51] also peaked in organic
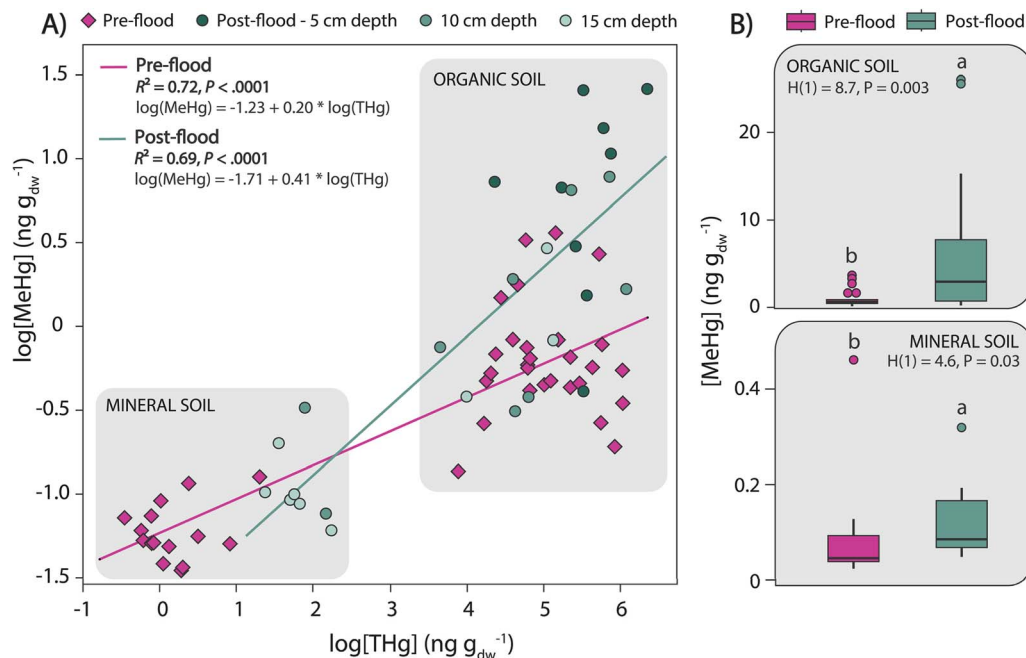
This journal is © The Royal Society of Chemistry 2025

Environ. Sci.: Processes Impacts, 2025, **27**, 3572–3585 | **3575**

Fig. 2 Total mercury and methylmercury in organic and mineral soils displayed as (A) the simple linear regression between log(MeHg) and log(THg) before (pink) and after (blue) the impoundment, with shades of blue representing different soil depths; and (B) boxplots of MeHg concentrations (ng g_{dw}^{-1}) before and after the impoundment.

soils, reaching an average of 3.0 ± 3.1%, which represents a near four-fold increase from 2022 (0.7 ± 0.6%).

Concentrations of THg (113 ± 23 ng g_{dw}^{-1}, $n = 9$) are comparable to those observed across northern regions,[52,53] but higher than lower latitudes regions found in the United States (mean of 24 ng g_{dw}^{-1}, $n = 1911$) and Europe (median of 40 ng g_{dw}^{-1}, $n = 1558$),[54] hence consolidating the growing presumption that permafrost regions store a significant amount of Hg.[16,17] THg's strong association with soil OM content is consistent with prior studies,[55] but the measured R_{HgC} of this study is more than six times lower than the R_{HgC} of 1.6 ± 0.9 µg Hg per g C used by Schuster et al. meta-analysis on permafrost soils.[17] The latter is based on 13 permafrost cores sampled along a latitudinal gradient in Alaska representing a broad array of characteristics and ages typical of circumpolar permafrost. Assuming that Hg concentrations in Alaska were representative of circumpolar permafrost Hg, they then upscaled median R_{HgC} to the circumpolar Arctic using published soil C maps from the Circumpolar Soil Carbon Database.[56] It therefore appears that median R_{HgC} coming from 13 cores from Alaska is not representative of R_{HgC} at our study site. Using these broadly derived estimates would have overestimated the amount of C and Hg that could be mobilized in our study area and probably in other regions of Nunavik with epigenetic permafrost.

Nevertheless, our results indicate that the impoundment of a small ROR in a northern tundra setting led to a near seven-fold increase of soil MeHg concentrations within three months. Bulk inorganic Hg readily available for uptake as well as OM content are among the main components affecting biotic methylation,[57] but interestingly not all samples displaying high carbon content nor high THg concentrations seemed to exhibit

higher % MeHg, which was rather influenced by the depth of soil. Flooded land experiences a rapid decomposition of fresh labile OM and can develop oxygen-deprived and reduced environments due to enhanced bacterial activity, thus creating ideal Hg methylation niches as well as the establishment of Hg methylators in new sediments.[58,59] Because the sediment–water interface often coincides with a strong redox gradient, this process as well as % MeHg tends to peak in the layer located a few centimetres below the water–sediment interface,[57,60,61] although this phenomenon has not been described in a permafrost area.

There are few studies on MeHg levels in flooded soils near RORs worldwide. One such study from southern Quebec on the St. Maurice River reported similar maximum MeHg levels (up to 20 ng g_{dw}^{-1}) and higher % MeHg (up to 12%) than those reported here, but with comparable mean values.[12] These values are lower than maximum ones reported for flooded soils in large scale reservoir systems. For instance, MeHg levels of up to 50 ng g_{dw}^{-1} have been reported in reservoirs from northern Quebec.[62] It is likely that higher temperature at lower latitudes may lead to higher net methylation, particularly in larger systems with extensive flooded areas. Furthermore, the flooding of permafrost soil in this study may be likened to what happens during permafrost thaw. For instance, Tarbier et al.[63] reported a 13-fold increase in % MeHg after the collapse of a fen (representing thawed conditions) as compared to a peat plateau (representing frozen conditions) in a subarctic environment. This is higher than the 4-fold increase we observed, likely because our study only encompasses the first 3 months post-flooding. Alternatively, it may reflect the fact that the organic layer containing most THg was thin at our site compared to the peat plateau.

3576 | Environ. Sci.: Processes Impacts, 2025, **27**, 3572–3585

This journal is © The Royal Society of Chemistry 2025

Overall, our results suggest that soil THg mainly resides in the organic fraction of the active layer, indicating that even if the flooding destabilized the underlying permafrost, it would likely not result in the release of large quantities of ice-immobilized Hg. The near-surface active layer response to the flooding is restricted to a small area and should reflect locally on the overlaying water.

Timeline of the flooding event reveals minimal impacts on riverine mercury exports

Apart from the two sites sampled post-flood in the newly created bay, the river exhibited consistently low concentrations of unfiltered THg and MeHg, averaging 0.58 ± 0.35 ng L^{-1} and 0.099 ± 0.178 ng L^{-1}, respectively. Bulk DOC averaged 2.90 ± 0.23 mg L^{-1}, with the highest concentrations monitored in the new bay followed by the spring high-flow. It correlated well with THg (Spearman's rho = 0.61, $p < 0.0001$) but not with MeHg (Spearman's rho = 0.03, $p = 0.87$), which maintained concentrations close to the detection limit throughout the whole campaign, except for two extreme points in the newly flooded bay. Furthermore, dissolved organic matter (DOM) showed a prominence of terrestrial-derived humic-like material as highlighted by the five-component parallel factor analysis (PARAFAC) model. In non-flooded sites, DOM quality was a better predictor of dissolved THg than bulk DOC, with the strongest predictive power obtained with terrestrial-derived humic-like components C1, C2 and C4 (Table S4). However, when adding the two extreme points from the newly flooded bay, bulk DOC was the strongest predictor. Overall, concentrations of aqueous DOC and THg, primarily the dissolved fraction, roughly tracked the river seasonal discharge fluctuations (DOC: $R^2 = 0.83$, $p < 0.0001$; dissolved THg: $R^2 = 0.73$, $p <$ 0.0001), as well as the discharge variations observed throughout the flooding event that spanned over several days, in the summer of 2023.

During the creation of the headpond, the initial increase in water level upstream from the plant decelerated the river flow until water surpassed the spillway, resulting in a rapid increase in the discharge downstream (Fig. 3). This surge was accompanied by about a doubling in terms of suspended particulate matter, from 1.3 to 2.6 mg L^{-1}, a short pulse that lasted for a day before decreasing to previous levels. In addition, the subsequent daily monitoring downstream from the spillway revealed a short-lived spike in THg and MeHg levels, especially apparent for the particulate fractions. The latter experienced the greatest variation within the first five days, with a relative standard deviation of 60% for particulate THg and 50% for particulate MeHg, before returning to prior levels within five days (Fig. 3). Moreover, the dissolved fractions peaked during the rising phase, while the maximal particulate THg concentration was measured during peak discharge, and interestingly particulate MeHg culminated during the falling discharge phase (Fig. 3).

All sampling campaigns combined, most of the dissolved C pool was characterized as modern with some samples exhibiting slightly older carbon, while all POC samples showed older radiocarbon age, ranging from 250 to 1130 years before present (BP). All records considered, the particulate fraction was slightly older ($\Delta^{14}C = -105 \pm 24‰$) than the dissolved one ($\Delta^{14}C = -20 \pm 34‰$), but no clear age-changing pattern could be established between surface water sampled before, during and after the flooding.

Riverine THg concentrations were in the lower range of previous data collected from large rivers in Nunavik,[64] whilst low MeHg concentrations are typical of arctic streams.[65] An alignment between stream discharge, terrestrial-derived DOM
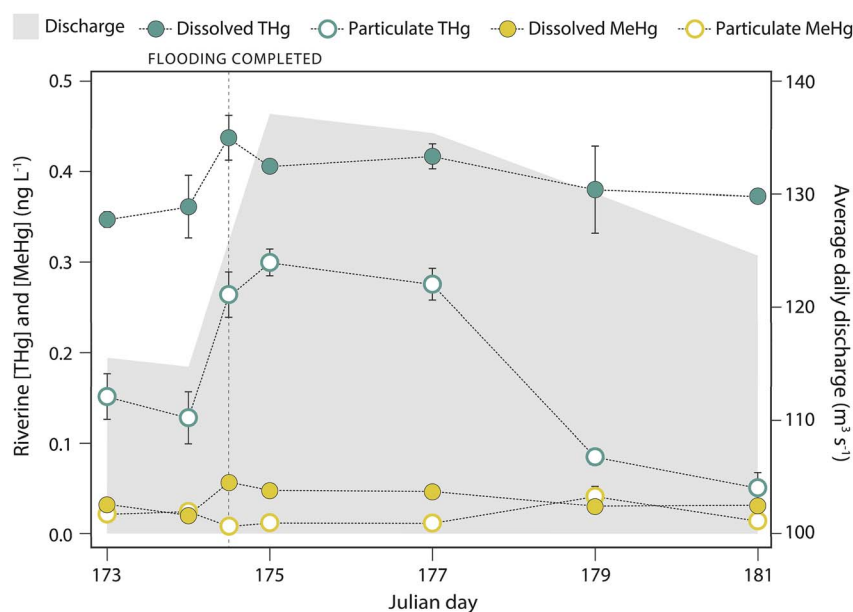

Fig. 3 Short term response of the dissolved (filled dots) and particulate (open dots) fractions of total mercury (green) and methylmercury (yellow) to the flooding event in June 2023 in contrast with the average daily flow rate (light grey).

This journal is © The Royal Society of Chemistry 2025

Environ. Sci.: Processes Impacts, 2025, **27**, 3572–3585 | **3577**

and THg concentrations is common since high flow is linked to either storm events or snowmelt-driven freshet, all of which typically lead to an episodic flush of soil fresh OM and associated compounds.[66–70] This flood event temporally promoted Hg transport, as the short-term spikes of THg and MeHg could be a function of the rapidly increased river flow.[30] The rise of the water level also most likely led to the implementation of an erosion regime at different soil depths, with surface erosion happening at first, which was previously associated with a bigger increase for the particulate fractions than for the dissolved ones, followed by deeper subsurface flow erosion.[71–73] Nonetheless, this event had minimal longer-term impact on Hg mobilisation as concentrations fell back to prior levels within a few days.

Aqueous methylmercury increases locally in the newly flooded bay

Three months post-flood, the flooded bay had MeHg concentrations (0.60 ± 0.38 ng L^{-1}) and % MeHg ($51 \pm 6\%$), respectively, 10 and four-fold higher than other sites along the river (0.05 ± 0.01 ng L^{-1}; $13 \pm 7\%$). Simple linear regression models run between % MeHg and DOC concentration or composition were weak (R^2 of the best model $= 0.16$). However, excluding the two extreme points corresponding to the newly flooded bay from the dataset improved some of the models. Concentrations of terrestrial humic-like C1 showed a significantly negative relationship with % MeHg ($R^2 = 0.53$, $p < 0.0001$), while the latter was positively related with the relative microbially derived humic-like % C3 ($R^2 = 0.52$, $p < 0.0001$) (Fig. 4). In addition, % C3 tended to increase throughout the year, with the highest values observed during the fall low flow of October 2023 (Fig. 4).

Those results suggest that the natural riverine Hg methylation processes of the undisturbed systems are hampered by humic-like allochthonous material loading, consistent with previous findings because these complex molecules are often recalcitrant to heterotrophic microbial processing.[74,75] While the autochthonous protein-like C5 component did not stand out in our analyses as previously observed,[76–78] the strong coupling between % C3 and % MeHg suggests that microbial processing is a good indicator of Hg methylation efficiency; proportion of C3, commonly interpreted as a terrestrial material that recently underwent microbial processing, as well as % MeHg both peaked at the end of the growing season, which often coincides with heightened microbial processing due to higher light exposure, warmer temperatures and extended water residence time.[46,79]

These findings also suggest a transitory shift in equilibrium in this newly formed reactive environment. The processes at play remain unclear but could imply unusual inputs of organic matter in the system, either originating from the flooded topsoils, where methylmercury production seems to have been heavily activated, from the fast development of periphyton and the decomposing vegetation or from a combination of those sources. Ultimately, this increased availability of MeHg in the system could have an impact on the aquatic biota that colonises this new methylation hotspot.
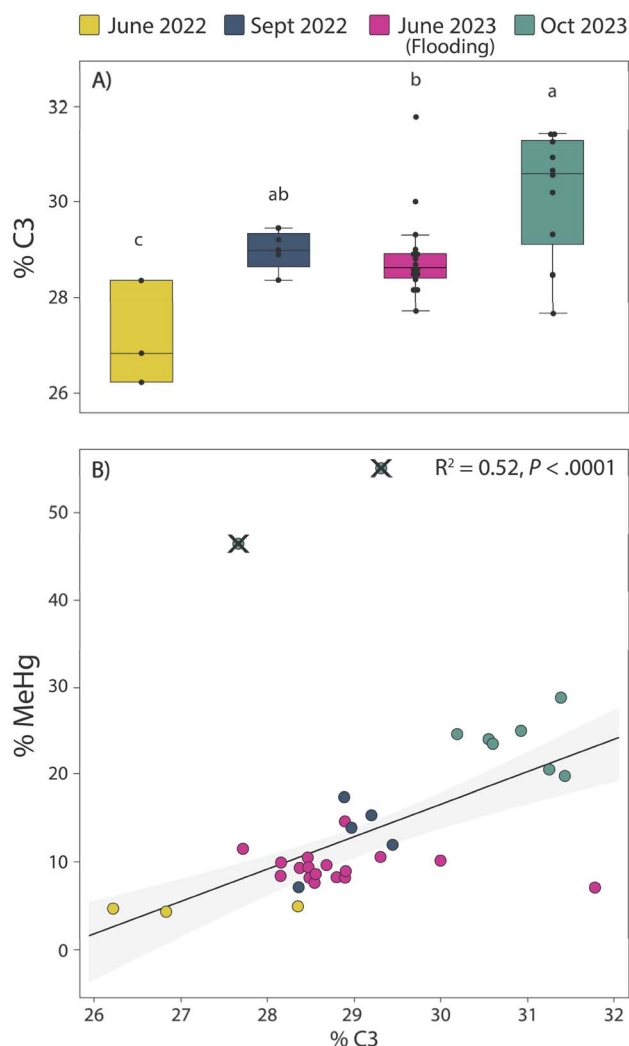

Fig. 4 Proportion of PARAFAC component C3 represented as (A) boxplots grouped by sampling period with the significant differences between groups showed by lowercase letters (Wilcoxon test: $p = 0.002$) and (B) its simple linear regression with % MeHg, with two extreme points corresponding to the newly flooded bay (X dots) shown but excluded from the model.

Three months of impoundment causes a rapid MeHg increase at the base of the food web in the flooded bay

When comparing the trophic groups pre- (2022) and post-impoundment (2023), significantly higher MeHg burdens were observed in post-impoundment primary consumers ($[MeHg]_{2022} = 35 \pm 12$ ng g^{-1}, $n = 35$; $[MeHg]_{2023} = 138 \pm 102$ ng g^{-1}; $p < 0.0001$) and omnivorous invertebrates ($[MeHg]_{2022} = 151 \pm 77$, $n = [MeHg]_{2023} = 430 \pm 103$, $n = 5$; $p = 0.0017$) but not in pelagic predators ($[MeHg]_{2022} = 375 \pm 73$, $n = 12$; $[MeHg]_{2023} = 351 \pm 206$, $n = 7$; $p = 0.252$). With only two juvenile slimy sculpins collected post-impoundment, no clear pattern could be drawn for small fishes, but those two individuals showed MeHg concentrations (476 ± 51 ng g^{-1}, $n = 2$) higher than the ones sampled in 2022 (158 ± 67 ng g^{-1}, $n = 15$) even though they belonged to the same size range.

3578 | Environ. Sci.: Processes Impacts, 2025, **27**, 3572–3585

This journal is © The Royal Society of Chemistry 2025

Additionally, within primary consumers sampled post-impoundment, a clear gradient of MeHg concentrations as well as more depleted δ^{13}C signatures was seen from the

flooded bay to downstream. While δ^{13}C, widely used to reconstruct dietary niches,[80] showed a significant negative relationship with MeHg concentrations (2022: $R^2 = 0.30$, $p <$
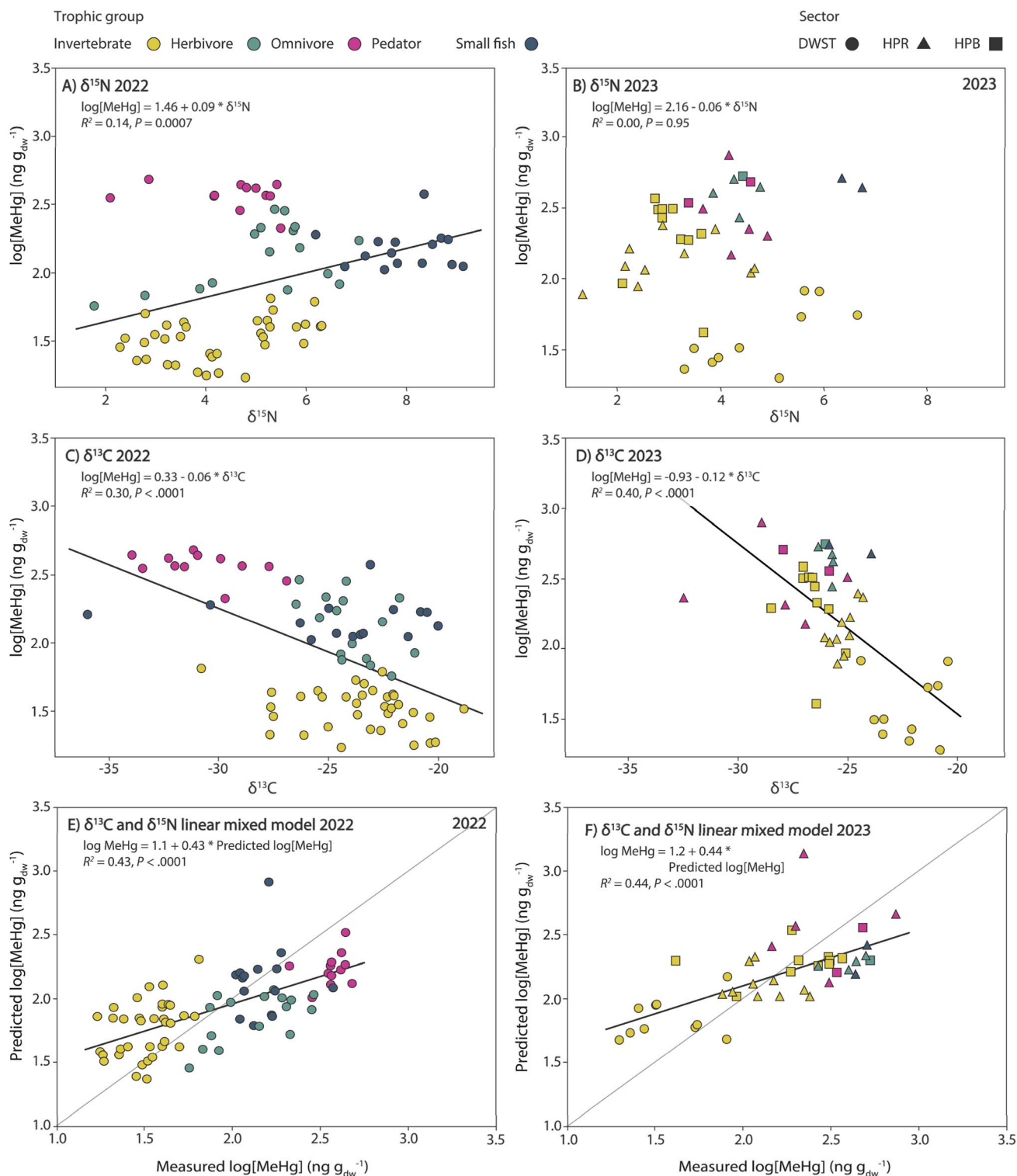
Fig. 5 Simple linear regressions of log[MeHg] (ng g_{dw}^{-1}) measured in biota plotted with δ^{15}N (‰, (A and B)) and δ^{13}C (‰, (C and D)) in pre-flood conditions of 2022 (left panels) and three months post-flood in 2023 (right panels), and predicted log[MeHg] from the δ^{13}C and δ^{15}N linear mixed model plotted with measured log[MeHg] (ng g_{dw}^{-1}) for 2022 (E) and 2023 (F). Trophic groups of invertebrates and small fishes are shown by the different colors while sampling sectors are highlighted by different shapes for the 2023 data only. A fit line is shown when the model is significant.

0.0001) (Fig. 5C) that strengthened post-flood ($R^2 = 0.40$, $p < 0.0001$) (Fig. 5D), the $\delta^{15}N$ signatures seemed completely decoupled from MeHg concentrations post-flood (2022: $R^2 = 0.14$, $p = 0.0007$; 2023: $R^2 = 0.00$, $p = 0.95$) (Fig. 5A and B). Furthermore, the use of a linear mixed model (LMM) using $\delta^{13}C$ and $\delta^{15}N$ bettered the predictive power for MeHg concentrations for 2022 ($R^2 = 0.43$, $p < 0.0001$) (Fig. 5E) and 2023 ($R^2 = 0.44$, $p < 0.0001$) (Fig. 5F). Finally, the pre-flood MeHg trophic magnification slope (TMS) was 0.09, resulting in a trophic magnification factor (TMF) of 2.03, meaning that MeHg doubles between each trophic level, but no TMS nor TMF could be estimated post-impoundment due to the lack of association between $\delta^{15}N$ and MeHg concentrations.

Many previous publications showed that the trophic position derived from nitrogen isotopic signatures was a strong predictor of MeHg accumulation,[80-82] but it was not the case in this study when all organisms were plotted together (Fig. 5A and B). However, in 2022 pre-flood conditions, the predator Notonectidae had the lowest and only significantly different $\delta^{13}C$ signature than other guilds (Wilcoxon test, $p < 0.0001$), which points to a possible reliance on an alternative carbon source as well as limited dietary interactions with the benthic food web (Fig. 5C). Lower $\delta^{13}C$ values can typically be indicators of pelagic food sources while in contrast, strong reliance on the benthic environment would be reflected by higher ones.[83,84] This corroborates the depleted $\delta^{13}C$ signatures measured in Notonectidae as they are pelagic predators, as compared to the fish species collected, mainly juvenile slimy sculpins, whose lack of swim bladder and small habitat range make them closely associated with bottom sediments.[85]

The pre-flood biomagnification potential of MeHg in our study system (TMS = 0.09) remained much beneath the average TMS for freshwater lotic systems (0.27 ± 0.08) reported in the global meta-analysis conducted by Lavoie *et al.* (2013),[6] which could be explained by the higher complexity of benthic food webs as benthic invertebrates may overlap in feeding strategies and feed at multiple trophic levels.[86] In this study, $\delta^{13}C$ signatures, widely used to reconstruct dietary niches,[80] displayed a stronger coupling with MeHg in tissues (Fig. 5C and D) in contrast with $\delta^{15}N$ (Fig. 5A and B), which is not uncommon for the assemblage of low-trophic organisms.[13,87] Both isotopic signatures remained however relevant to explain MeHg variability, as the LMM incorporating both variables provided the best fit for the data (Fig. 5E and F).

In addition, the strengthened relationship between MeHg burdens and $\delta^{13}C$ post-impoundment (Fig. 5C and D) further supports that bioaccumulation at this low trophic level range is highly influenced by C sources rather than by trophic dynamics. This is also supported by the highest MeHg concentrations measured in primary consumers collected in the newly flooded bay, where $\delta^{13}C$ was the most depleted (Fig. 5D). Lower $\delta^{13}C$ values were previously observed in the flooded area of a boreal ROR and were attributed to the heightened C processing of fresh OM,[13] which favours MeHg production. Furthermore, the lack of a relationship between MeHg concentrations and $\delta^{15}N$ observed post-flood could indicate that there is a certain delay in MeHg trophic transfer that was not reached within three

months, which supports previous findings from the Mercury Experiment To Assess Atmospheric Loading In Canada and the United States, where the food web of an experimentally Hg-spiked lake did not reach biomagnification equilibrium before 5 years.[88]

Therefore, our results highlight an enhanced biological uptake of MeHg three months post-impoundment in the first links of the benthic food chain, particularly evident for invertebrates sampled in the newly flooded bay, where $\delta^{13}C$ signatures were stronger predictors of MeHg bioaccumulation than $\delta^{15}N$.

Conclusions

This study provides short-term insights on the biogeochemical impacts of a first ROR built in remote sub-arctic features, which are expected to increase in the future. We found that Hg rich soils were limited to the permafrost active layer, and that the Hg stocks in this area are very likely lower than those suggested by previous global estimates, hence suggesting that global estimates of the soil Hg : C ratio should be used with caution in understudied areas. Overall, the topsoil of the newly created flooded bay showed an enhanced Hg methylation efficiency three months post-impoundment. This increased activity was reflected in surface waters as well as in low trophic level organisms closely associated with the benthic environment, but these effects seemed locally restricted to the small <1 km² flooded bay. Furthermore, we observed that high flow events are an important source of soil particles associated with a greater input of co-transported inorganic Hg. In contrast, the production of MeHg seems greater towards the end of the growing season where the low flow is more suitable for carbon processing by the microbial communities. These observations were supported by carbon processing indicators such as higher % C3 in surface waters and depleted $\delta^{13}C$ signatures in biota, which proved to be useful to predict methylation efficiency and MeHg bioaccumulation, respectively. This study suggests that run-of-river reservoirs in permafrost areas can have noticeable effects on Hg at the local scale; future studies should determine if these new Hg hotspots in the riverscape will result in a transient contamination of the upper food web, particularly if fish populations are attracted by this new habitat. Considering our results, future northern development of run-of-river power plants should integrate a biomonitoring plan for Hg even if only a small area is flooded.

Conflicts of interest

Jeanne Gaudreault is a retired employee of Innergex Renewable Energy.

Data availability

The data supporting this article have been included as part of the supplementary information (SI). Supplementary information is available. See DOI: **https://doi.org/10.1039/d5em00171d**.

3580 | *Environ. Sci.: Processes Impacts*, 2025, **27**, 3572–3585

This journal is © The Royal Society of Chemistry 2025

Acknowledgements

References

1 S. Kelly-Richards, N. Silber-Coats, A. Crootof, D. Tecklin and C. Bauer, Governing the Transition to Renewable Energy: A Review of Impacts and Policy Issues in the Small Hydropower Boom, *Energy Policy*, 2017, 251–264, DOI: 10.1016/j.enpol.2016.11.035.

2 T. B. A. Couto, M. L. Messager and J. D. Olden, Safeguarding Migratory Fish via Strategic Planning of Future Small Hydropower in Brazil, *Nat. Sustain.*, 2021, **4**(5), 409–416, DOI: 10.1038/s41893-020-00665-4.

3 T. Ptak, A. Crootof, T. Harlan and S. Kelly, Critically Evaluating the Purported Global "Boom" in Small Hydropower Development through Spatial and Temporal Analysis, *Renew. Sustain. Energy Rev.*, 2022, **163**, 112490, DOI: 10.1016/j.rser.2022.112490.

4 M. Amyot, F. Bilodeau, A. Tremblay, D. Planas, D. Walsh and D. E. Ponton, Cumulative Effects of Watershed Disturbances and Run-of-River Dams on Mercury Cycling: Case Study and Recommendations for Environmental Managers, *Environ. Manag.*, 2024, DOI: 10.1007/s00267-024-01990-6.

5 M. Premalatha, T. Abbasi, T. Abbasi and S. A. Abbasi, A Critical View on the Eco-Friendliness of Small Hydroelectric Installations, *Sci. Total Environ.*, 2014, **481**(1), 638–643, DOI: 10.1016/j.scitotenv.2013.11.047.

6 R. A. Lavoie, T. D. Jardine, M. M. Chumchal, K. A. Kidd and L. M. Campbell, Biomagnification of Mercury in Aquatic Food Webs: A Worldwide Meta-Analysis, *Environ. Sci. Technol.*, 2013, **47**(23), 13385–13394, DOI: 10.1021/es403103t.

7 R. Schetagne and J. Therrien, *Environmental Monitoring at the La Grande Complex Evolution of Fish Mercury Levels*, 2013.

8 T. B. A. Couto and J. D. Olden, Global Proliferation of Small Hydropower Plants – Science and Policy, *Front. Ecol. Environ.*, 2018, 91–100, DOI: 10.1002/fee.1746.

9 E. C. Cebalho, S. Díez, M. dos Santos Filho, C. C. Muniz, W. Lázaro, O. Malm and A. R. A. Ignácio, Effects of Small Hydropower Plants on Mercury Concentrations in Fish, *Environ. Sci. Pollut. Res.*, 2017, **24**(28), 22709–22716, DOI: 10.1007/s11356-017-9747-1.

10 W. R. Bastos, J. G. Dórea, L. D. Lacerda, R. Almeida, W. A. Costa-Junior, C. C. Baía, I. F. Sousa-Filho, E. A. Sousa, I. A. S. Oliveira, C. S. Cabral, A. G. Manzatto, D. P. Carvalho, K. A. N. Ribeiro and O. Malm, Dynamics of Hg and MeHg in the Madeira River Basin (Western Amazon) before and after Impoundment of a Run-of-River Hydroelectric Dam, *Environ. Res.*, 2020, **189**, 109896, DOI: 10.1016/j.envres.2020.109896.

11 V. M. Silverthorn, C. A. Bishop, T. Jardine, J. E. Elliott and C. A. Morrissey, Impact of Flow Diversion by Run-of-River Dams on American Dipper Diet and Mercury Exposure, *Environ. Toxicol. Chem.*, 2018, **37**(2), 411–426, DOI: 10.1002/etc.3961.

12 L. Millera Ferriz, D. E. Ponton, V. Storck, M. Leclerc, F. Bilodeau, D. A. Walsh and M. Amyot, Role of Organic Matter and Microbial Communities in Mercury Retention and Methylation in Sediments near Run-of-River Hydroelectric Dams, *Sci. Total Environ.*, 2021, **774**, 145686, DOI: 10.1016/j.scitotenv.2021.145686.

13 D. E. Ponton, R. A. Lavoie, M. Leclerc, F. Bilodeau, D. Planas and M. Amyot, Understanding Food Web Mercury Accumulation through Trophic Transfer and Carbon Processing along a River Affected by Recent Run-of-River Dams, *Environ. Sci. Technol.*, 2021, **55**(5), 2949–2959, DOI: 10.1021/acs.est.0c07015.

14 M. Leclerc, D. E. Ponton, F. Bilodeau, D. Planas and M. Amyot, Enhanced Bioaccumulation and Transfer of Monomethylmercury through Periphytic Biofilms in Benthic Food Webs of a River Affected by Run-of-River Dams, *Environ. Sci. Technol.*, 2023, **57**(49), 20792–20801, DOI: 10.1021/acs.est.3c05585.

15 A. Dastoor, H. Angot, J. Bieser, J. H. Christensen, T. A. Douglas, L. E. Heimbürger-Boavida, M. Jiskra, R. P. Mason, D. S. McLagan, D. Obrist, P. M. Outridge, M. V. Petrova, A. Ryjkov, K. A. St. Pierre, A. T. Schartup, A. L. Soerensen, K. Toyota, O. Travnikov, S. J. Wilson and C. Zdanowicz, Arctic Mercury Cycling, *Nat. Rev. Earth Environ.*, 2022, 270–286, DOI: 10.1038/s43017-022-00269-w.

16 A. G. Lim, M. Jiskra, J. E. Sonke, S. V. Loiko, N. Kosykh and O. S. Pokrovsky, A Revised Pan-Arctic Permafrost Soil Hg Pool Based on Western Siberian Peat Hg and Carbon Observations, *Biogeosciences*, 2020, 3083–3097, DOI: 10.5194/bg-17-3083-2020.

17 P. F. Schuster, K. M. Schaefer, G. R. Aiken, R. C. Antweiler, J. F. Dewild, J. D. Gryziec, A. Gusmeroli, G. Hugelius, E. Jafarov, D. P. Krabbenhoft, L. Liu, N. Herman-Mercer, C. Mu, D. A. Roth, T. Schaefer, R. G. Striegl, K. P. Wickland and T. Zhang, Permafrost Stores a Globally Significant Amount of Mercury, *Geophys. Res. Lett.*, 2018, **45**(3), 1463–1471, DOI: 10.1002/2017GL075571.

18 Y. Wang, G. Shi, D. Wang, Q. Zhao, S. Jiang, Y. Li, D. Wang, C. Li, Z. Chen and R. Bargagli, Relationships between Concentrations of Mercury and Organic Carbon in Soils Allow the Identification of Antarctic Ice-Free Areas with

This journal is © The Royal Society of Chemistry 2025

Environ. Sci.: Processes Impacts, 2025, **27**, 3572–3585 | **3581**

Enhanced Deposition of the Metal, *Catena*, 2023, **220**, 106718, DOI: **10.1016/J.CATENA.2022.106718**.

19 R. A. Lavoie, M. Amyot and J. F. Lapierre, Global Meta-Analysis on the Relationship Between Mercury and Dissolved Organic Carbon in Freshwater Environments, *J. Geophys. Res.:Biogeosci.*, 2019, **124**(6), 1508–1523, DOI: **10.1029/2018JG004896**.

20 G. L. Lescord, E. J. S. Emilson, T. A. Johnston, B. A. Branfireun and J. M. Gunn, Optical Properties of Dissolved Organic Matter and Their Relation to Mercury Concentrations in Water and Biota Across a Remote Freshwater Drainage Basin, *Environ. Sci. Technol.*, 2018, **52**(6), 3344–3353, DOI: **10.1021/acs.est.7b05348**.

21 J. B. Shanley, V. F. Taylor, K. A. Ryan, A. T. Chalmers, J. Perdrial and A. Stubbins, Using Dissolved Organic Matter Fluorescence to Predict Total Mercury and Methylmercury in Forested Headwater Streams, Sleepers River, Vermont USA, *Hydrol. Process.*, 2022, **36**(5), e14572, DOI: **10.1002/hyp.14572**.

22 K. Bishop, J. B. Shanley, A. Riscassi, H. A. de Wit, K. Eklöf, B. Meng, C. Mitchell, S. Osterwalder, P. F. Schuster, J. Webster and W. Zhu, Recent Advances in Understanding and Measurement of Mercury in the Environment: Terrestrial Hg Cycling, *Sci. Total Environ.*, 2020, **721**, 137647, DOI: **10.1016/J.SCITOTENV.2020.137647**.

23 K. Schaefer, Y. Elshorbany, E. Jafarov, P. F. Schuster, R. G. Striegl, K. P. Wickland and E. M. Sunderland, Potential Impacts of Mercury Released from Thawing Permafrost, *Nat. Commun.*, 2020, **11**(1), 4650, DOI: **10.1038/s41467-020-18398-5**.

24 K. R. Miner, J. D'Andrilli, R. Mackelprang, A. Edwards, M. J. Malaska, M. P. Waldrop and C. E. Miller, Emergent Biogeochemical Risks from Arctic Permafrost Degradation, *Nat. Clim. Change*, 2021, **11**(10), 809–819, DOI: **10.1038/s41558-021-01162-y**.

25 P. Godin, R. W. Macdonald, Z. Z. A. Kuzyk, M. A. Goñi and G. A. Stern, Organic Matter Compositions of Rivers Draining into Hudson Bay: Present-Day Trends and Potential as Recorders of Future Climate Change, *J. Geophys. Res.:Biogeosci.*, 2017, **122**(7), 1848–1869, DOI: **10.1002/2016JG003569**.

26 A. Campeau, K. Eklöf, A. L. Soerensen, S. Åkerblom, S. Yuan, H. Hintelmann, M. Bieroza, S. Köhler and C. Zdanowicz, Sources of Riverine Mercury across the Mackenzie River Basin; Inferences from a Combined Hg–C Isotopes and Optical Properties Approach, *Sci. Total Environ.*, 2022, **806**(Part 4), 150808, DOI: **10.1016/j.scitotenv.2021.150808**.

27 K. J. McFarlane, H. M. Throckmorton, J. M. Heikoop, B. D. Newman, A. L. Hedgpeth, M. N. Repasch, T. P. Guilderson and C. J. Wilson, Age and Chemistry of Dissolved Organic Carbon Reveal Enhanced Leaching of Ancient Labile Carbon at the Permafrost Thaw Zone, *Biogeosciences*, 2022, **19**(4), 1211–1223, DOI: **10.5194/bg-19-1211-2022**.

28 M. Wauthy, M. Rautio, K. S. Christoffersen, L. Forsström, I. Laurion, H. L. Mariash, S. Peura and W. F. Vincent, Increasing Dominance of Terrigenous Organic Matter in Circumpolar Freshwaters Due to Permafrost Thaw, *Limnol. Oceanogr. Lett.*, 2018, **3**(3), 186–198, DOI: **10.1002/lol2.10063**.

29 L. Zheng, I. Overeem, K. Wang and G. D. Clow, Changing Arctic River Dynamics Cause Localized Permafrost Thaw, *J. Geophys. Res.: Earth Surf.*, 2019, **124**(9), 2324–2344, DOI: **10.1029/2019JF005060**.

30 M. T. K. Tsui, J. D. Blum and S. Y. Kwon, Review of Stable Mercury Isotopes in Ecology and Biogeochemistry, *Sci. Total Environ.*, 2020, **716**, 135386, DOI: **10.1016/J.SCITOTENV.2019.135386**.

31 Pituvik Landholding Corporation and Innergex, *Innavik Hydroelectric Project Environmental and Social Impact Assessment Summary*, 2019.

32 P. Lajeunesse, Early Holocene Deglaciation of the Eastern Coast of Hudson Bay, *Geomorphology*, 2008, **99**(1–4), 341–352, DOI: **10.1016/J.GEOMORPH.2007.11.012**.

33 P. Lajeunesse and M. Allard, Late Quaternary Deglaciation, Glaciomarine Sedimentation and Glacioisostatic Recovery in the Rivière Nastapoka Area, Eastern Hudson Bay, Northern Québec, *Géogr. Phys. Quaternaire*, 2003, **57**(1), 65–83, DOI: **10.7202/010331ar**.

34 J. A. Heginbottom, M. A. Dubreuil and P. T. Harker, Canada, permafrost, in *The National Atlas of Canada*, MCR Series 4177, Natural Resources Canada, Geomatics Canada, 5th edn, 1995, DOI: **10.4095/294672**.

35 A. B. St-Amour, M. Allard, A. Chiasson, S. Aubé-Michaud, V. Mathon-Dufour, E. L. Hérault, S. Bilodeau and C. Deslauriers, *Caractérisation Géotechnique et Cartographie Améliorée Du Pergélisol Dans Les Communautés Nordiques Du Nunavik Inukjuak Ministère Des Affaires Municipales et de l'Habitation, Gouvernement Du Québec. Rapport Final*, Centre d'études Nordiques, Université Laval, Québec, 2020, p. 120.

36 V. St Louis, J. W. Rudd, C. A. Kelly, K. G. Beaty, N. S. Bloom and R. J. Flett, Importance of Wetlands as Sources of Methyl Mercury To, *Can. J. Fish. Aquat. Sci.*, 1994, **51**, 1065–1076.

37 Environmental Protection Agency, *EPA Method 7473 (SW-846): Mercury in Solids and Solutions by Thermal Decomposition, Amalgamation, and Atomic Absorption Spectrophotometry*, 2007.

38 Environmental Protection Agency, *Method 1631, Revision E: Mercury in Water by Oxidation, Purge and Trap, and Cold Vapor Atomic Fluorescence Spectrometry*, 2002.

39 Environmental Protection Agency, *Method 1630: Methyl Mercury in Water by Distillation, Aqueous Ethylation, Purge and Trap, and Cold Vapor Atomic Fluorescence Spectrometry*, 1998.

40 C. Fink-Mercier, J. F. Lapierre, M. Amyot and P. A. del Giorgio, Concentrations and Yields of Total Hg and MeHg in Large Boreal Rivers Linked to Water and Wetland Coverage in the Watersheds, *J. Geophys. Res.:Biogeosci.*, 2022, **127**(5), e2022JG006892, DOI: **10.1029/2022JG006892**.

41 W. E. Dean, Determination of Carbonate and Organic Matter in Calcareous Sediments and Sedimentary Rocks by Loss on Ignition; Comparison with Other Methods, *J. Sediment. Res.*, 1974, **44**(1), 242–248, DOI: **10.1306/74D729D2-2B21-11D7-8648000102C1865D**.

3582 | *Environ. Sci.: Processes Impacts*, 2025, **27**, 3572–3585

This journal is © The Royal Society of Chemistry 2025

42 Soil Classification Working Group, *The Canadian System of Soil Classification*, Agric. and Agri-Food Can., 3rd edn, 1998.

43 Environmental Protection Agency, *Total Organic Carbon in Water EPA Method 415.1 (Combustion or Oxidation)*, 1999.

44 J. De Bonville, M. Amyot, P. del Giorgio, A. Tremblay, F. Bilodeau, D. E. Ponton and J. F. Lapierre, Mobilization and Transformation of Mercury Across a Dammed Boreal River Are Linked to Carbon Processing and Hydrology, *Water Resour. Res.*, 2020, **56**(10), e2020WR027951, DOI: **10.1029/2020WR027951**.

45 K. R. Murphy, C. A. Stedmon, P. Wenig and R. Bro, OpenFluor- An Online Spectral Library of Auto-Fluorescence by Organic Compounds in the Environment, *Anal. Methods*, 2014, **6**(3), 658–661, DOI: **10.1039/c3ay41935e**.

46 S. Shousha, R. Maranger and J. F. Lapierre, Contrasting Seasons and Land Uses Alter Riverine Dissolved Organic Matter Composition, *Biogeochemistry*, 2022, **161**(2), 207–226, DOI: **10.1007/s10533-022-00979-9**.

47 C. A. Crann, S. Murseli, G. St-Jean, X. Zhao, I. D. Clark and W. E. Kieser, First Status Report on Radiocarbon Sample Preparation Techniques at the A.E. Lalonde AMS Laboratory (Ottawa, Canada), *Radiocarbon*, 2017, **59**, 695–704, DOI: **10.1017/RDC.2016.55**.

48 S. Murseli, P. Middlestead, G. St-Jean, X. Zhao, C. Jean, C. A. Crann, W. E. Kieser and I. D. Clark, The Preparation of Water (DIC, DOC) and Gas (CO 2, CH 4) Samples for Radiocarbon Analysis at AEL-AMS, Ottawa, Canada, *Radiocarbon*, 2019, **61**(5), 1563–1571, DOI: **10.1017/rdc.2019.14**.

49 A. R. Millard, Conventions for Reporting Radiocarbon Determinations, *Radiocarbon*, 2014, **56**(2), 555–559, DOI: **10.2458/56.17455**.

50 T. Frohne, J. Rinklebe, U. Langer, G. Du Laing, S. Mothes and R. Wennrich, Biogeochemical Factors Affecting Mercury Methylation Rate in Two Contaminated Floodplain Soils, *Biogeosciences*, 2012, **9**(1), 493–507, DOI: **10.5194/bg-9-493-2012**.

51 J. Liu, D. Wang, J. Zhang, V. Liem-Nguyen, R. Huang and T. Jiang, Evaluation of Hg Methylation in the Water-Level-Fluctuation Zone of the Three Gorges Reservoir Region by Using the MeHg/HgT Ratio, *Ecotoxicol. Environ. Saf.*, 2020, **195**, 110468, DOI: **10.1016/J.ECOENV.2020.110468**.

52 C. Olson, M. Jiskra, H. Biester, J. Chow and D. Obrist, Mercury in Active-Layer Tundra Soils of Alaska: Concentrations, Pools, Origins, and Spatial Distribution, *Global Biogeochem. Cycles*, 2018, **32**(7), 1058–1073, DOI: **10.1029/2017GB005840**.

53 K. Halbach, Ø. Mikkelsen, T. Berg and E. Steinnes, The Presence of Mercury and Other Trace Metals in Surface Soils in the Norwegian Arctic, *Chemosphere*, 2017, **188**, 567–574, DOI: **10.1016/J.CHEMOSPHERE.2017.09.012**.

54 C. Ballabio, M. Jiskra, S. Osterwalder, P. Borrelli, L. Montanarella and P. Panagos, A Spatial Assessment of Mercury Content in the European Union Topsoil, *Sci. Total Environ.*, 2021, **769**, 144755, DOI: **10.1016/J.SCITOTENV.2020.144755**.

55 J. B. Richardson, A. J. Friedland, T. R. Engerbretson, J. M. Kaste and B. P. Jackson, Spatial and Vertical Distribution of Mercury in Upland Forest Soils across the Northeastern United States, *Environ. Pollut.*, 2013, **182**, 127–134, DOI: **10.1016/J.ENVPOL.2013.07.011**.

56 G. Hugelius, J. Strauss, S. Zubrzycki, J. W. Harden, E. A. G. Schuur, C.-L. Ping, L. Schirrmeister, G. Grosse, G. J. Michaelson, C. D. Koven, J. A. O'Donnell, B. Elberling, U. Mishra, P. Camill, Z. Yu, J. Palmtag and P. Kuhry, Estimated Stocks of Circumpolar Permafrost Carbon with Quantified Uncertainty Ranges and Identified Data Gaps, *Biogeosciences*, 2014, **11**(23), 6573–6593, DOI: **10.5194/bg-11-6573-2014**.

57 S. M. Ullrich, T. W. Tanton and S. A. Abdrashitova, Mercury in the Aquatic Environment: A Review of Factors Affecting Methylation, *Crit. Rev. Environ. Sci. Technol.*, 2001, 241–293, DOI: **10.1080/20016491089226**.

58 K. Eklöf, P. Drohan, J. Needoba, S. Landefeld, T. D. Peterson, H. Hu, L. Iavorivska and E. W. Boyer, Methylmercury in Lake Bed Soils during Re-Flooding of an Appalachian Reservoir in the Northeastern Usa, *Environ. Res. Commun.*, 2021, **3**(8), 085004, DOI: **10.1088/2515-7620/ac1d83**.

59 C. Lawruk-Desjardins, V. Storck, D. E. Ponton, M. Amyot and D. A. Walsh, A Genome Catalogue of Mercury-Methylating Bacteria and Archaea from Sediments of a Boreal River Facing Human Disturbances, *Environ. Microbiol.*, 2024, **26**(6), e16669, DOI: **10.1111/1462-2920.16669**.

60 B. D. Hall, V. L. St. Louis, K. R. Rolfhus, R. A. Bodaly, K. G. Beaty, M. J. Paterson and K. A. P. Cherewyk, Impacts of Reservoir Creation on the Biogeochemical Cycling of Methyl Mercury and Total Mercury in Boreal Upland Forests, *Ecosystems*, 2005, **8**(3), 248–266, DOI: **10.1007/s10021-003-0094-3**.

61 B. Meng, X. Feng, G. Qiu, Z. Li, H. Yao, L. Shang and H. Yan, The Impacts of Organic Matter on the Distribution and Methylation of Mercury in a Hydroelectric Reservoir in Wujiang River, Southwest China, *Environ. Toxicol. Chem.*, 2016, **35**(1), 191–199, DOI: **10.1002/etc.3181**.

62 M. Lucotte, R. Schetagne, N. Thérien, C. Langlois and C. Langlois, *Mercury in the Biogeochemical Cycle – Natural Environments and Hydroelectric Reservoirs of Northern Québec (Canada)*, Springer Berlin Heidelberg, Berlin, Heidelberg, 1st edn, 1999, DOI: **10.1007/978-3-642-60160-6**.

63 B. Tarbier, G. Hugelius, A. B. K. Sannel, C. Baptista-Salazar and S. Jonsson, Permafrost Thaw Increases Methylmercury Formation in Subarctic Fennoscandia, *Environ. Sci. Technol.*, 2021, **55**(10), 6710–6717, DOI: **10.1021/acs.est.0c04108**.

64 M. Wauthy, M. Amyot, D. E. Ponton, C. Fink-Mercier, F. Bilodeau, A. Tremblay, P. del Giorgio and J. F. Lapierre, Riverine Exports of Mercury and Methylmercury from Dammed and Undammed Rivers of Quebec, Eastern Canada, *Estuar. Coast Shelf Sci.*, 2023, **284**, 108272, DOI: **10.1016/J.ECSS.2023.108272**.

65 J. Chételat, M. Amyot, P. Arp, J. M. Blais, D. Depew, C. A. Emmerton, M. Evans, M. Gamberg, N. Gantner, C. Girard, J. Graydon, J. Kirk, D. Lean, I. Lehnherr,

This journal is © The Royal Society of Chemistry 2025

Environ. Sci.: Processes Impacts, 2025, **27**, 3572–3585 | **3583**

D. Muir, M. Nasr, A. J. Poulain, M. Power, P. Roach, G. Stern, H. Swanson and S. van der Velden, Mercury in Freshwater Ecosystems of the Canadian Arctic: Recent Advances on Its Cycling and Fate, *Sci. Total Environ.*, 2015, 41–66, DOI: **10.1016/j.scitotenv.2014.05.151**.

66 M. Derrien, M. H. Lee, K. Choi, K. S. Lee and J. Hur, Tracking the Evolution of Particulate Organic Matter Sources during Summer Storm Events via End-Member Mixing Analysis Based on Spectroscopic Proxies, *Chemosphere*, 2020, **252**, 126445, DOI: **10.1016/J.CHEMOSPHERE.2020.126445**.

67 L. Gandois, N. I. Tananaev, A. Prokushkin, I. Solnyshkin and R. Teisserenc, Seasonality of DOC Export From a Russian Subarctic Catchment Underlain by Discontinuous Permafrost, Highlighted by High-Frequency Monitoring, *J. Geophys. Res.:Biogeosci.*, 2021, **126**(10), e2020JG006152, DOI: **10.1029/2020JG006152**.

68 B. N. Packer, G. T. Carling, T. J. Veverica, K. A. Russell, S. T. Nelson and Z. T. Aanderud, Mercury and Dissolved Organic Matter Dynamics during Snowmelt Runoff in a Montane Watershed, Provo River, Utah, USA, *Sci. Total Environ.*, 2020, **704**, 135297, DOI: **10.1016/J.SCITOTENV.2019.135297**.

69 L. M. Thompson, M. Low, R. Shewan, C. Schulze, M. Simba, O. Sonnentag, S. E. Tank and D. Olefeldt, Concentrations and Yields of Mercury, Methylmercury, and Dissolved Organic Carbon From Contrasting Catchments in the Discontinuous Permafrost Region, Western Canada, *Water Resour. Res.*, 2023, **59**(11), e2023WR034848, DOI: **10.1029/2023WR034848**.

70 Z. Wu, Z. Li, B. Shao, Y. Zhang, W. He, Y. Lu, K. Gusvitskii, Y. Zhao, Y. Liu, X. Wang and Y. Tong, Impact of Dissolved Organic Matter and Environmental Factors on Methylmercury Concentrations across Aquatic Ecosystems Inferred from a Global Dataset, *Chemosphere*, 2022, **294**, 133713, DOI: **10.1016/J.CHEMOSPHERE.2022.133713**.

71 X. Liu, X. Lu, R. Yu, H. Sun, Y. Li, Z. Qi, H. Xue, Z. Zhang, Z. Cao, T. Liu and C. Lu, Sediment and Carbon Dynamics during an Episodic Flood in an Intermittent River, *Ecosphere*, 2022, **13**(10), e4248, DOI: **10.1002/ecs2.4248**.

72 H. G. Sun, J. T. Han, S. R. Zhang and X. X. Lu, The Impacts of "05.6" Extreme Flood Event on Riverine Carbon Fluxes in Xijiang River, *Chin. Sci. Bull.*, 2007, **52**(6), 805–812, DOI: **10.1007/s11434-007-0111-6**.

73 T. N. Wiegner, R. L. Tubal and R. A. MacKenzie, Bioavailability and Export of Dissolved Organic Matter from a Tropical River during Base- And Stormflow Conditions, *Limnol. Oceanogr.*, 2009, **54**(4), 1233–1242, DOI: **10.4319/lo.2009.54.4.1233**.

74 P. Massicotte and J.-J. Frenette, Spatial Connectivity in a Large River System: Resolving the Sources and Fate of Dissolved Organic Matter, *Ecol. Appl.*, 2011, **21**(7), 2600–2617, DOI: **10.1890/10-1475.1**.

75 H. Xu and L. Guo, Intriguing Changes in Molecular Size and Composition of Dissolved Organic Matter Induced by Microbial Degradation and Self-Assembly, *Water Res.*, 2018, **135**, 187–194, DOI: **10.1016/J.WATRES.2018.02.016**.

76 A. G. Bravo, D. N. Kothawala, K. Attermeyer, E. Tessier, P. Bodmer, J. L. J. Ledesma, J. Audet, J. P. Casas-Ruiz, N. Catalán, S. Cauvy-Fraunié, M. Colls, A. Deininger, V. V. Evtimova, J. A. Fonvielle, T. Fuß, P. Gilbert, S. H. Ortega, L. Liu, C. Mendoza-Lera, J. Monteiro, J. R. Mor, M. Nagler, G. H. Niedrist, A. C. Nydahl, A. Pastor, J. Pegg, C. G. Roberts, F. Pilotto, A. P. Portela, C. R. González-Quijano, F. Romero, M. Rulík and D. Amouroux, The Interplay between Total Mercury, Methylmercury and Dissolved Organic Matter in Fluvial Systems: A Latitudinal Study across Europe, *Water Res.*, 2018, **144**, 172–182, DOI: **10.1016/J.WATRES.2018.06.064**.

77 T. Jiang, A. G. Bravo, U. Skyllberg, E. Björn, D. Wang, H. Yan and N. W. Green, Influence of Dissolved Organic Matter (DOM) Characteristics on Dissolved Mercury (Hg) Species Composition in Sediment Porewater of Lakes from Southwest China, *Water Res.*, 2018, **146**, 146–158, DOI: **10.1016/J.WATRES.2018.08.054**.

78 S. Noh, J. Kim, J. Hur, Y. Hong and S. Han, Potential Contributions of Dissolved Organic Matter to Monomethylmercury Distributions in Temperate Reservoirs as Revealed by Fluorescence Spectroscopy, *Environ. Sci. Pollut. Res.*, 2018, **25**(7), 6474–6486, DOI: **10.1007/s11356-017-0913-2**.

79 H. J. Dalmagro, M. S. Johnson, C. R. de Musis, M. J. Lathuillière, J. Graesser, O. B. Pinto-Júnior and E. G. Couto, Spatial Patterns of DOC Concentration and DOM Optical Properties in a Brazilian Tropical River-Wetland System, *J. Geophys. Res.:Biogeosci.*, 2017, **122**(8), 1883–1902, DOI: **10.1002/2017JG003797**.

80 C. McClelland, J. Chételat, K. Conlan, A. Aitken, M. R. Forbes and A. Majewski, Methylmercury Dietary Pathways and Bioaccumulation in Arctic Benthic Invertebrates of the Beaufort Sea, *Arct. Sci.*, 2024, **10**(2), 305–320, DOI: **10.1139/as-2023-0021**.

81 H. A. De Wit, M. J. Kainz and M. Lindholm, Methylmercury Bioaccumulation in Invertebrates of Boreal Streams in Norway: Effects of Aqueous Methylmercury and Diet Retention, *Environ. Pollut.*, 2012, **164**, 235–241, DOI: **10.1016/j.envpol.2012.01.041**.

82 M. W. Swinton, P. K. Myer, M. F. Schaller, E. A. Pettitt, J. L. Farrell and S. A. Nierzwicki-Bauer, Stable Carbon and Nitrogen Isotopes Explain Methylmercury Concentrations in Stream Food Webs of Lake George, New York (USA), *Ecotoxicology*, 2022, **31**(5), 808–821, DOI: **10.1007/s10646-022-02548-0**.

83 M. A. Bradford, M. L. Mallory and N. J. O'Driscoll, Ecology and Environmental Characteristics Influence Methylmercury Bioaccumulation in Coastal Invertebrates, *Chemosphere*, 2024, **346**, 140502, DOI: **10.1016/j.chemosphere.2023.140502**.

84 J. P. Coelho, C. L. Mieiro, E. Pereira, A. C. Duarte and M. A. Pardal, Mercury Biomagnification in a Contaminated Estuary Food Web: Effects of Age and Trophic Position Using Stable Isotope Analyses, *Mar. Pollut. Bull.*, 2013, **69**(1–2), 110–115, DOI: **10.1016/J.MARPOLBUL.2013.01.021**.

3584 | *Environ. Sci.: Processes Impacts*, 2025, **27**, 3572–3585

This journal is © The Royal Society of Chemistry 2025

85 M. A. Gray, R. Allen Curry, T. J. Arciszewski, K. R. Munkittrick and S. M. Brasfield, The Biology and Ecology of Slimy Sculpin: A Recipe for Effective Environmental Monitoring, *Facets*, 2018, 103–127, DOI: **10.1139/facets-2017-0069**.

86 I. R. Hilgendag, H. K. Swanson, C. W. Lewis, A. D. Ehrman and M. Power, Mercury Biomagnification in Benthic, Pelagic, and Benthopelagic Food Webs in an Arctic Marine Ecosystem, *Sci. Total Environ.*, 2022, **841**, 156424, DOI: **10.1016/j.scitotenv.2022.156424**.

87 M. Díaz-Jaramillo, C. Muñoz, I. Rudolph, M. Servos and R. Barra, Seasonal Mercury Concentrations and Δ15N and Δ13C Values of Benthic Macroinvertebrates and Sediments from a Historically Polluted Estuary in South Central Chile, *Sci. Total Environ.*, 2013, **442**, 198–206, DOI: **10.1016/j.scitotenv.2012.10.039**.

88 P. J. Blanchfield, J. W. M. Rudd, L. E. Hrenchuk, M. Amyot, C. L. Babiarz, K. G. Beaty, R. A. D. Bodaly, B. A. Branfireun, C. C. Gilmour, J. A. Graydon, B. D. Hall, R. C. Harris, A. Heyes, H. Hintelmann, J. P. Hurley, C. A. Kelly, D. P. Krabbenhoft, S. E. Lindberg, R. P. Mason, M. J. Paterson, C. L. Podemski, K. A. Sandilands, G. R. Southworth, V. L. St Louis, L. S. Tate and M. T. Tate, Experimental Evidence for Recovery of Mercury-Contaminated Fish Populations, *Nature*, 2022, **601**(7891), 74–78, DOI: **10.1038/s41586-021-04222-7**.

This journal is © The Royal Society of Chemistry 2025

Environ. Sci.: Processes Impacts, 2025, **27**, 3572–3585 | **3585**